Signal propagation in time-dependent spin transport

Yao-Hui Zhu, Burkard Hillebrands, and Hans Christian Schneider*
Physics Department and Research Center OPTIMAS, Kaiserslautern University of Technology, 67653 Kaiserslautern, Germany
(Received 20 June 2008; revised manuscript received 25 July 2008; published 20 August 2008)

This paper analyzes theoretically the signal propagation in spin transport by modulating the current passing through magnetic multilayers. Using a macroscopic description of spin transport based on the dynamical Boltzmann equation, we show that time-dependent spin transport possesses a wavelike character that leads to modifications of pure spin-diffusion dynamics. In particular, the wavelike characteristics allow one to extract a finite spin signal-propagation velocity.

DOI: 10.1103/PhysRevB.78.054429 PACS number(s): 72.25.−b, 75.40.Gb, 75.47.−m, 85.75.−d

I. INTRODUCTION

Time-dependent spin transport in magnetic multilayers with current perpendicular to the plane (CPP) is studied because of its significance in physics and promising applications in spintronics devices.[1,2] Most theoretical investigations are based on a diffusion equation for the spin accumulation or magnetization.[3–6] These theories show that if one drives a spin-polarized current through an interface from a magnetic to a nonmagnetic metallic layer, the spin propagates by "diffusing" into the nonmagnetic layers. If one considers time-dependent spin transport, such as spin transfer torque switching,[3,5] alternating current (AC),[4] or magnetization switching,[6] where a time-dependent signal is encoded in the spin orientation, one faces a difficulty of the diffusion equation in that no propagation velocity for the spin signal in the nonmagnetic layer can be defined. Stated differently, the diffusion equation yields an infinite propagation velocity for the spin signal in the nonmagnetic layer because the signal will appear everywhere as soon as the source is switched on.[3] In this paper, we show how a physical propagation velocity for spin signals in the CPP configuration can be determined by deriving and analyzing macroscopic dynamical equations for spin transport.

It is an interesting connection that a problem analogous to that of an infinite signal-propagation velocity in the spin-diffusion equation exists for the heat diffusion equation, which yields an infinite heat-conduction velocity. This difficulty was resolved by recognizing that the theoretical description of heat transport needs to be generalized by substituting the Maxwell-Cattaneo equation[7,8] for Fourier's law. In this way, one obtains the physical picture that heat conduction is characterized by a wave-diffusion duality. Formally, the heat diffusion equation needs to be replaced by an equation that is essentially a telegraph equation.[9,10] As we show in this paper, a similar modification of the spin-diffusion equation is necessary in the case of spin transport.

We base our derivation of the macroscopic equations for spin transport through multilayers on the theory developed for steady-state spin transport across magnetic multilayers by Valet and Fert.[11] Instead of using the time-independent Boltzmann equation as in Ref. 11, we treat time-dependent spin transport starting from the dynamical Boltzmann equation, which allows us to derive macroscopic equations and to generalize the spin-diffusion equation.

This paper is organized as follows. The macroscopic dynamical equations are derived in Sec. II of our paper. Since the central equations [Eqs. (18) and (19)] can also be cast in a form that resembles telegraph equations, we discuss qualitative aspects of dynamical spin transport in Sec. III using these telegraph equations. In Sec. IV, we analyze two concrete examples of time-dependent spin transport numerically, and the main conclusions are summarized in Sec. V.

II. TIME-DEPENDENT EQUATION SYSTEM

In this section, the model of Valet and Fert[11] for spin-dependent transport of conduction electrons through metallic multilayers will be extended to take into account the time dependence of spin transport. The electron distribution function $f_s(z,\mathbf{v},t)$ satisfies the linearized Boltzmann equation,

$$\frac{\partial f_s(z,\mathbf{v},t)}{\partial t} + v_z\frac{\partial f_s(z,\mathbf{v},t)}{\partial z} - eE(z,t)v_z\frac{\partial f^0(v)}{\partial \varepsilon}$$
$$= \int d^3v'\,\delta[\varepsilon(v') - \varepsilon(v)]P_s[z,\varepsilon(v)]$$
$$\times[f_s(z,\mathbf{v}',t) - f_s(z,\mathbf{v},t)]$$
$$+ \int d^3v'\,\delta[\varepsilon(v') - \varepsilon(v)]P_{sf}[z,\varepsilon(v)]$$
$$\times[f_{-s}(z,\mathbf{v}',t) - f_s(z,\mathbf{v},t)], \quad (1)$$

where $-e$ and $\varepsilon(v)=mv^2/2$ denote, respectively, the charge and kinetic energy of the electrons and $E(z,t)=-\partial V(z,t)/\partial z$ is the local electric field.[12] $P_s(z,\varepsilon)$ and $P_{sf}(z,\varepsilon)$ are the spin conserving and spin-flip transition probabilities, respectively. Following Ref. 11, we assume $f_s(z,\mathbf{v},t)$ to be the sum of the Fermi-Dirac distribution $f^0(v)$ and small perturbations,

$$f_s(z,\mathbf{v},t) = f^0(v) + \frac{\partial f^0}{\partial \varepsilon}\{[\mu^0 - \mu_s(z,t)] + g_s(z,\mathbf{v},t)\}, \quad (2)$$

where $\mu^0=mv_F^2/2$ and $\mu_s(z,t)$ are the equilibrium and nonequilibrium chemical potentials, respectively. Due to the cylindrical symmetry of the system around the z axis, $g_s(z,\mathbf{v},t)$ can be expanded in Legendre polynomials of cos θ, where θ is the angle between $\mathbf{v}$ and the z axis, as

$$g_s(z,\mathbf{v},t) = \sum_{n=1}^{\infty} g_s^{(n)}(z,t) P_n(\cos\,\theta). \tag{3}$$

Here, the zero-order (isotropic) term is absent because $(\partial f^0/\partial\varepsilon)g_s(z,\mathbf{v},t)$ was defined by Eq. (2) as the *anisotropic* part of the electron distribution perturbation. Using Eq. (3), we obtain

$$\frac{\partial g_s(z,\mathbf{v},t)}{\partial t} + v_z\frac{\partial g_s(z,\mathbf{v},t)}{\partial z} + \left(\frac{1}{\tau_s} + \frac{1}{\tau_{\rm sf}}\right) g_s(z,\mathbf{v},t) = \frac{\partial \mu_s(z,t)}{\partial t} + v_z\frac{\partial \bar{\mu}_s(z,t)}{\partial z} + \frac{\bar{\mu}_s(z,t) - \bar{\mu}_{-s}(z,t)}{\tau_{\rm sf}}, \tag{4}$$

where $\bar{\mu}_s(z,t) = \mu_s(z,t) - eV(z,t)$ is the electrochemical potential for electrons with spin s. The derivation of this equation is detailed in Appendix A2. Note that $\mathbf{v}$ in Eq. (4) has been restricted to the Fermi velocity v_F, i.e., $|\mathbf{v}| = v_F$ and $v_z = v_F \cos\,\theta$.

With the relaxation times τ_s and $\tau_{\rm sf}$ [see Eqs. (A9) and (A10) in Appendix A2], the local electron mean-free path λ_s, diffusion constant D_s, and spin-diffusion length l_s can be defined, respectively, as $\lambda_s = v_F\tau_s'$, $D_s = v_F\lambda_s/3$, and $l_s = (D_s\tau_{\rm sf})^{1/2}$, where the momentum relaxation time τ_s' is defined by

$$1/\tau_s' = 1/\tau_s + 1/\tau_{\rm sf}. \tag{5}$$

The appropriate "average" spin-diffusion length $l_{\rm sf}$ can be defined as $(1/l_{\rm sf})^2 = (1/l_+)^2 + (1/l_-)^2$. Throughout the paper, subscripts + and − stand for the *absolute* spin directions "up" and "down," respectively, whereas subscripts ↑ and ↓ stand for the majority- and minority-spin directions, respectively.

Using the method of Appendix B in Ref. 11, we express the time-dependent current density for spin s as

$$J_s(z,t) = -\frac{e}{V}\sum_{\mathbf{v}} f_s(z,\mathbf{v},t) v_z = \kappa g_s^{(1)}(z,t), \tag{6}$$

where $\kappa = \sigma_s/(e\lambda_s)$. Note that κ is independent of s and of the material in the Valet-Fert model. The conductivity σ_s can be written as $\sigma_s = e^2 n_s \tau_s'/m$, where $n_s = 4\pi(mv_F/h)^3/3$ is the number of electrons with spin s. It is easy to see that σ_s satisfies Einstein's relation $\sigma_s = e^2 N_s D_s$, where

$$N_s = \frac{1}{4\pi^2}(2m/\hbar^2)^{3/2}\sqrt{\mu^0} \tag{7}$$

is the density of states for spin s at the Fermi level μ^0, and $N_+ = N_-$.

Substituting Eqs. (3) and (6) into Eq. (4), we obtain

$$\frac{e}{\sigma_s}\frac{\partial J_s(z,t)}{\partial z} - \frac{1}{D_s}\frac{\partial \mu_s(z,t)}{\partial t} = \frac{\bar{\mu}_s(z,t) - \bar{\mu}_{-s}(z,t)}{l_s^2}, \tag{8}$$

$$J_s(z,t) = \frac{\sigma_s}{e}\frac{\partial \bar{\mu}_s(z,t)}{\partial z} - \tau_s'\frac{\partial J_s(z,t)}{\partial t}. \tag{9}$$

In steady state, $J_s(z,t)$ and $\bar{\mu}_s(z,t)$ become time independent and then Eqs. (8) and (9) reduce to Eqs. (10) and (11) of Ref. 11, respectively.

Equations (8) and (9) will be transformed to more directly usable forms next. Without loss of generality, the magnetization of the ferromagnet is set to be up. Then, the majority (minority) spins, which are antiparallel (parallel) to the local magnetization [electron magnetic moment is $\boldsymbol{\mu} = -(e/m)\mathbf{s}$] and denoted by subscript ↑ (↓), point to the absolute spin direction down (up) denoted by subscript − (+). In terms of $J_m(z,t) = J_+(z,t) - J_-(z,t)$ and $\mu_m(z,t) = \mu_+(z,t) - \mu_-(z,t)$, Eqs. (8) and (9) can be written as

$$\frac{\partial J_m(z,t)}{\partial z} - eN_s\frac{\partial \mu_m(z,t)}{\partial t} = eN_s\frac{\mu_m(z,t)}{T_1}, \tag{10}$$

$$J_m(z,t) = eN_s\bar{D}\frac{\partial \mu_m(z,t)}{\partial z} - \tau\frac{\partial J_m(z,t)}{\partial t} - \tilde{\beta}J(z,t), \tag{11}$$

where

$$T_1 = \tau_{\rm sf}/2 \tag{12}$$

can be regarded as the spin-relaxation time.[13] The average diffusion constant $\bar{D}$ is defined as $\bar{D} = c^2\tau$, with the wavefront velocity c defined by

$$c^2 = v_F^2/3. \tag{13}$$

The average momentum relaxation time τ is

$$1/\tau = (1/\tau_+' + 1/\tau_-')/2, \tag{14}$$

and we have the identity $l_{\rm sf} = c\sqrt{\tau T_1}$. In Eq. (11), $\tilde{\beta} = (\tau_- - \tau_+')/(\tau_-' + \tau_+')$ equals β and 0 for the ferromagnetic and nonmagnetic layers, respectively. The bulk spin asymmetry coefficient β in the ferromagnetic layer is defined by $\rho_{\uparrow(\downarrow)} = 1/\sigma_{\uparrow(\downarrow)} = 2\rho_F^*[1-(+)\beta]$, where ρ_F^* is the total resistivity of the ferromagnetic layer. In the nonmagnetic layer, we have $\rho_{\uparrow(\downarrow)} = 2\rho_N^*$, where ρ_N^* is the total resistivity of the nonmagnetic layer.

In Eq. (11), $J(z,t)$ stands for the total current density, $J(z,t) = J_+(z,t) + J_-(z,t)$. By introducing $\mu(z,t) = [\mu_+(z,t) + \mu_-(z,t)]/2$, we can also derive equations for the charge dynamics,

$$\frac{\partial J(z,t)}{\partial z} - 2eN_s\frac{\partial \mu(z,t)}{\partial t} = 0, \tag{15}$$

$$J(z,t) = 2eN_s\bar{D}\frac{\partial}{\partial z}[\mu(z,t) - eV(z,t)] - \tau\frac{\partial J(z,t)}{\partial t} - \tilde{\beta}J_m(z,t). \tag{16}$$

To describe spin accumulation by spin density instead of the chemical potential, it is necessary to transform Eqs. (10) and (11) using the following identity [Eq. (A15)]:

$$n_m(z,t) = -eN_s\mu_m(z,t), \tag{17}$$

where $n_m(z,t) = n_+(z,t) - n_-(z,t)$ is the spin density and $n_s(z,t)$ the nonequilibrium charge density for spin s. Using Eq. (17), we can rewrite Eqs. (10) and (11) as

$$\frac{\partial J_m(z,t)}{\partial z} + \frac{\partial n_m(z,t)}{\partial t} = -\frac{n_m(z,t)}{T_1}, \tag{18}$$

$$J_m(z,t) = -\bar{D}\frac{\partial n_m(z,t)}{\partial z} - \tau\frac{\partial J_m(z,t)}{\partial t} - \tilde{\beta}J(z,t). \quad (19)$$

To proceed further, we need the following identity [Eq. (A16)]:

$$n(z,t) - 2n_s^0 = -eN_s[2\mu(z,t) - 2\mu^0], \quad (20)$$

where $n(z,t)=n_+(z,t)+n_-(z,t)$ is total nonequilibrium charge density and n_s^0 the equilibrium charge density for spin s. Using Eq. (20), we can rewrite Eqs. (15) and (16) as

$$\frac{\partial J(z,t)}{\partial z} + \frac{\partial n(z,t)}{\partial t} = 0, \quad (21)$$

$$J(z,t) = -\bar{D}\frac{\partial n(z,t)}{\partial z} - 2e^2N_s\bar{D}\frac{\partial V(z,t)}{\partial z} - \tau\frac{\partial J(z,t)}{\partial t} - \tilde{\beta}J_m(z,t). \quad (22)$$

In general, Eqs. (18) and (19) should be solved together with Eqs. (21) and (22), and Poisson's equation. However, in metals and degenerate semiconductors, the accumulation of charge occurs on a much smaller length scale and varies much faster than that of spin.[3–6] Thus as an approximation, it is assumed that the charge accumulation described by $n(z,t)$ can always reach its steady state instantaneously when spin transport is considered. This means that we always set $\partial n(z,t)/\partial t=0$, which leads to $\partial J(z,t)/\partial z=0$ according to Eq. (21). Therefore, the current density $J(z,t)$ in Eqs. (11) and (19) becomes independent of z and can be written as $J(t)$ instead.

III. "TELEGRAPH" EQUATION

In order to see the physical significance of the dynamics described by Eqs. (18) and (19) and to compare it with the spin-diffusion equation used in Refs. 3–6 we combine Eqs. (18) and (19) to yield the following equations:

$$\frac{\partial^2 n_m(z,t)}{\partial t^2} + \left(\frac{1}{\tau}+\frac{1}{T_1}\right)\frac{\partial n_m(z,t)}{\partial t} + \frac{n_m(z,t)}{\tau T_1} = c^2\frac{\partial^2 n_m(z,t)}{\partial z^2}, \quad (23)$$

$$\frac{\partial^2 J_m(z,t)}{\partial t^2} + \left(\frac{1}{\tau}+\frac{1}{T_1}\right)\frac{\partial J_m(z,t)}{\partial t} + \frac{J_m(z,t)}{\tau T_1} = c^2\frac{\partial^2 J_m(z,t)}{\partial z^2} - \tilde{\beta}\left[\frac{1}{\tau}\frac{\partial J(t)}{\partial t} + \frac{J(t)}{\tau T_1}\right]. \quad (24)$$

Because of the formal similarity of each of Eqs. (23) and (24) with the telegraph equation, we will refer to them as telegraph equations in the following.

Each of the telegraph equations contains a second-order time derivative, which is absent in the spin-diffusion equation. This term originates from the time derivative of the spin current in Eq. (19), which is also absent in the corresponding equation for the spin current in spin-diffusion theory [see, for instance, Eq. (8) of Ref. 3]. This additional term shows that it takes a finite time for the spin current to adjust to the gradient of the spin accumulation.[9,14] The second-order time and space derivatives lead to a wave character of dynamical spin transport in addition to its diffusion character described by the first-order time and second-order space derivatives. Thus, these equations show that time-dependent spin transport should be understood using a wave-diffusion duality picture. The occurrence of *spin accumulation waves* enables one to determine a well-defined propagation velocity c for the signal in time-dependent spin transport. Although the spin-diffusion equation does not yield spin accumulation waves and thus a finite signal-propagation velocity, it can be regarded as an approximation of the wave-diffusion duality of the time-dependent spin transport in the long-time limit.

In the following, the telegraph equation of the nonmagnetic layer will be analyzed in detail. Here, we have $\tau=\tau_s'$ and $\tilde{\beta}=0$. Thus, Eqs. (23) and (24) have the same structure and we discuss only Eq. (23) without loss of generality. We seek a damped and dispersive wave solution to Eq. (23) of the form

$$n_m(z,t) = n_m^0 \exp[i(kz-\omega t)]. \quad (25)$$

At this stage, we can set either $\omega=\omega_r+i\omega_i$ or $k=k_r+ik_i$. The complex ω and k will yield damping factors in time and space, respectively. Since we are more interested in the damping length (or the dynamical spin-diffusion length), we will follow the method of Ref. 15 and assume $k=k_r+ik_i$. Substituting Eq. (25) into Eq. (23), we get the dispersion relation,

$$-\omega^2 - i\alpha\omega + \xi = -c^2k^2, \quad (26)$$

where $\alpha=1/\tau_s'+1/T_1$ and $\xi=1/(\tau_s'T_1)$. Separating the real and imaginary parts of Eq. (26), we obtain

$$k_{r,i}^2 = \frac{1}{2c^2}[\sqrt{(\omega^2-\xi)^2+\alpha^2\omega^2} \pm (\omega^2-\xi)]. \quad (27)$$

The wavelength, defined as $2\pi/|k_r|$, can be written as

$$\frac{\lambda}{\lambda_{s,z}} = 2\pi\sqrt{2}[\sqrt{(\tilde{\omega}^2-\eta)^2+(\eta+1)^2\tilde{\omega}^2}+(\tilde{\omega}^2-\eta)]^{-1/2}, \quad (28)$$

where $\lambda_{s,z}=c\tau_s'$ is the z component of the electron mean-free path. Moreover, we have introduced dimensionless quantities,

$$\tilde{\omega} = \omega\tau_s', \quad \eta = \tau_s'/T_1. \quad (29)$$

The damping length, defined as $l_d=1/|k_i|$, can be written as

$$\frac{l_d}{\lambda_{s,z}} = \sqrt{2}[\sqrt{(\tilde{\omega}^2-\eta)^2+(\eta+1)^2\tilde{\omega}^2}-(\tilde{\omega}^2-\eta)]^{-1/2}. \quad (30)$$

Note that l_d can also be regarded as the dynamical spin-diffusion length. When $\tilde{\omega}\to 0$ or ∞, the damping length l_d will approach l_{sf} or $2l_{\mathrm{sf}}\sqrt{\tau_s'T_1}/(\tau_s'+T_1)$, respectively.

Figure 1 shows the variation of $l_d/\lambda_{s,z}$ and $\lambda/\lambda_{s,z}$ with $\omega\tau_s'$ for three different values of η. Note that the curves of $\lambda/\lambda_{s,z}$ for different η are very close to each other in the frequency range shown in the figure. The damping length l_d decreases

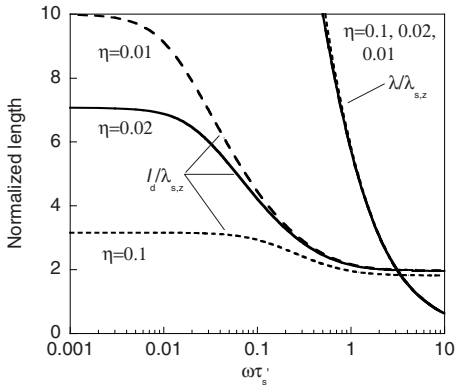

FIG. 1. Variation of $l_d/\lambda_{s,z}$ and $\lambda/\lambda_{s,z}$ with $\omega\tau_s'$ for three different values of η. The short-dashed, solid, and long-dashed curves correspond to η=0.1, 0.02, and 0.01, respectively.

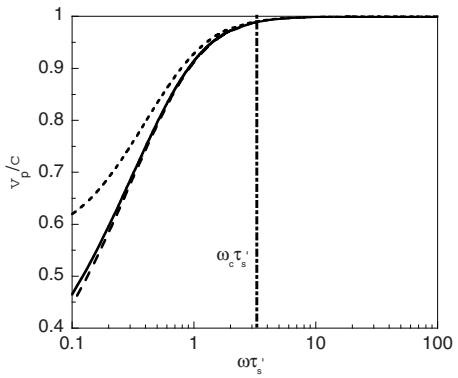

FIG. 2. Variation of v_p/c with $\omega\tau_s'$ for three different values of η. The short-dashed, solid, and long-dashed curves correspond to η=0.1, 0.02, and 0.01, respectively. The thick vertical dot-dashed line indicates the critical angular frequencies $\omega_c\tau_s'$ for the three different values of η, which are very close to each other according to Eq. (31).

with frequency, which is analogous to the skin effect of the electromagnetic wave propagating in metal. The intersection of $l_d/\lambda_{s,z}$ and $\lambda/\lambda_{s,z}$ indicates the critical angular frequency ω_c, which separates the wavelike region from the diffusion dominated regime, because the wave character becomes significant only if the damping length exceeds the wavelength. Stated differently, the wave character is significant if the typical time scale τ_{sig} of the time-dependent process is smaller than the critical period $T_c=2\pi/\omega_c$. On the contrary, the diffusion character is dominant if $\tau_{\mathrm{sig}}>T_c$, and the spin-diffusion picture becomes a good approximation of the wave-diffusion duality in the limit $\tau_{\mathrm{sig}}\gg T_c$.

An explicit expression for the critical angular frequency ω_c is obtained by combining $\lambda=l_d$ with Eq. (27)

$$\omega_c\tau_s' = \frac{1}{2}[\gamma(1+\eta) + \sqrt{\gamma^2(1+\eta)^2 + 4\eta}] \approx \gamma + \left(\gamma + \frac{1}{\gamma}\right)\eta, \tag{31}$$

where $\gamma=\pi-1/(4\pi)\approx 3.06$. Then, we have $\omega_c\tau_s'=3.06+3.4\eta$ approximately.

The phase velocity, defined as $v_p=\omega/|k_r|$, of the spin accumulation wave can be written as

$$\frac{v_p}{c} = \frac{\sqrt{2}}{\eta+1}[\sqrt{(\tilde{\omega}^2-\eta)^2 + (\eta+1)^2\tilde{\omega}^2} - (\tilde{\omega}^2-\eta)]^{1/2}. \tag{32}$$

When $\tilde{\omega}\to 0$ or ∞, the phase velocity v_p approaches $2c/(\eta^{1/2}+\eta^{-1/2})$ or c, respectively. When $\eta=1$, the phase velocity becomes equal to c for all frequencies. Furthermore, the group velocity can be defined as $v_g=d\omega/dk_r$ and calculated from Eq. (26).

Figure 2 shows the phase velocity v_p as functions of $\tilde{\omega}$ for η=0.1, 0.02, and 0.01. The phase velocity is approximately equal to the wave-front velocity c when the wave character is significant ($\omega>\omega_c$). In this case, the phase velocity provides a good description of the wavelike dynamics. On the contrary, when the wave character is insignificant ($\omega<\omega_c$), the wave amplitude is damped strongly and the phase velocity is not meaningful anymore. In this region, the propagation velocity is the wave-front velocity c, albeit only on the length scale of a damping length.

In the special case where $\eta=1$ ($\tau_s'=T_1$), we have $|k_r|=\omega/c$ and $|k_i|=1/l_{\mathrm{sf}}$. This means that the spin accumulation wave becomes a nondispersive but dissipative wave with the constant phase (and group) velocity c and penetration depth l_{sf}. However, this case is likely not realized because T_1 is usually much larger than τ_s' and Valet-Fert theory is justified to be valid only when $(\tau_s'/2T_1)^{1/2}\ll 1$.

IV. NUMERICAL RESULTS

In this section, the general analysis of the telegraph equations for spin transport is augmented by numerical solutions for two illustrative examples of signal propagation using spin-polarized currents through a ferromagnet/metal junction: (i) injection of an alternating current and (ii) instantaneous magnetization switching. The results are obtained by numerically solving the system of Eqs. (10) and (11). Our numerical method is outlined in Appendix A4. These equations are equivalent to the telegraph equations [Eqs. (23) and (24)], which have been discussed in Sec. III, but are easier to solve. Alternatively, we could solve the equation system consisting of Eqs. (18) and (19), in which the spin accumulation is described by the spin density. However, it is more convenient to work with the electrochemical potential than the spin density when we deal with the boundary conditions.[19]

We choose a ferromagnet/metal junction consisting of Co and Cu as the material system in both of the scenarios. The interface of the junction is placed at $z=0$ and the Co (Cu) occupies the half-space $z>0$ ($z<0$). The positive direction of the current is parallel to the positive direction of the z axis. For simplicity, the interface resistance of the junction will be neglected. Then, the electrochemical potential and the current density are continuous across the interface. Consequently, the spin transport across two layers can be described by one common equation system with different material parameters for the two layers.

TABLE I. Parameters for Cu and Co used in numerical calculation. The units of v_F, $\rho^*_{N(F)}$, and $l^{N(F)}_{\mathrm{sf}}$ are nm/ps, Ω nm, and nm, respectively. τ and T_1 are given in ps.

Material	v_F	$\rho^*_{N(F)}$	$l^{N(F)}_{\mathrm{sf}}$	$\tilde{\beta}$	τ	T_1
Cu	1570[a]	6[b]	450[b]	0	0.07[e]	3.5[e]
Co	1570[a]	86[c]	60[d]	0.5[c]	0.005[e]	0.9[e]

[a]From Ref. 16; Cu and Co are assumed to have a common Fermi velocity in the Valet-Fert model.
[b]From Ref. 17.
[c]From Ref. 11.
[d]From Ref. 18.
[e]Calculated from Eqs. (12) and (14).

The material parameters used in our numerical calculation are shown in Table I. All other parameters can be obtained from the values in Table I. In particular, the wave-front velocity is calculated to be $c=910$ nm/ps from Eq. (13). In the nonmagnetic layer, $\eta=\tau_s'/T_1=0.02$. The wavelength λ and damping length l_d are shown as the solid curves in Fig. 1. The critical period T_c can be estimated to be $2\tau_s' \simeq 0.14$ ps from Eq. (31), and the phase velocity is plotted in Fig. 2.

A. AC injection

The alternating charge current density passing through the ferromagnet/metal junction is assumed to be of the form $J(t)=J_0 \sin(\omega t)$, where $J_0=100$ nA/nm^2. Note that the z dependence of the charge current $J(z,t)$ in Eq. (11) is neglected for the investigation of the spin transport as pointed out in Sec. II. Two typical frequencies are studied in the case of the AC drive, $\nu_a=\omega_a/(2\pi)=8.33$ THz and $\nu_b=\omega_b/(2\pi)=0.23$ THz, which are larger and smaller than the critical frequency $\nu_c=\omega_c/(2\pi)=7.11$ THz, of Cu, respectively. The corresponding periods of the two frequencies are $T_a=0.12$ ps and $T_b=4.4$ ps, which satisfy $T_a<T_c<T_b$. The numerical results for the two frequencies are discussed in the following.

High-frequency case ($\omega=\omega_a>\omega_c$). Figure 3 shows snapshots of the spin-current density $J_m(z,t)$ at times $t=1.75T_a$ and $t=5.75T_a$. At both times, the charge current density $J(t)$ reaches its minimum $J(t)=-J_0$. The wave front, i.e., the spin signal, can be seen clearly in Fig. 3(a), where the time t is so small that the wave front has not propagated beyond the scale of the damping length l_d. In Fig. 3(b), the signal has propagated further, and due to the attenuation of the wave, the wave front is less clearly visible. Nevertheless, the wave-front velocity c can be determined numerically (or experimentally) by tracking the motion of the wave front over a short-time interval after switching on the drive current. Since we are using a signal time scale shorter than the critical time, we expect from the analysis in Sec. III (see also Fig. 2) the phase velocity to be $v_p \simeq c=910$ nm/ps from Eq. (13) and a wavelength $\lambda=108$ nm. These expectations are borne out by the numerical results. The dynamical damping length l_d can also be extracted from the numerical data, or from an experiment, by fitting a decay time to the envelope of the spin-current signal for longer times. Due to inaccuracies of the fitting procedure, this quantity is more difficult to determine quantitatively but agrees well with the damping length $l_d=126$ nm expected from Eq. (30). An important qualitative conclusion can be drawn by comparing the decay of the dynamical spin signal in Fig. 3(b) with the spin-current density $J_m(z)$ that results from a constant current density $J=-J_0$, which is also shown. Since our dynamical equations and the spin-diffusion equation have the same long-time limit, the DC result is identical with steady-state spin diffusion. It is apparent that the damping length l_d becomes much shorter than the spin-diffusion length l_{sf} of the steady-state spin transport with DC bias. This is the "skin" effect, which is already present in the analytical results in Sec. III.

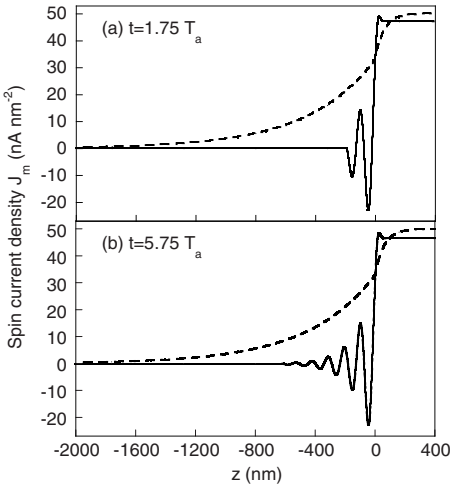

FIG. 3. Spin-current density $J_m(z,t)$ as a function of z. The solid curves in (a) and (b) are $J_m(z,t)$ at $t=1.75T_a$ and $t=5.75T_a$ [charge current $J(t)=-J_0$] with AC drive, respectively. The dashed curves in (a) and (b) are the spin-current density $J_m(z)$ resulting from the dc density, $J=-J_0$.

Figure 4 shows the z-dependent spin accumulation μ_m for the same parameters as in Fig. 3(b). The wavelength, damping length, and phase velocity given by Fig. 4 are very similar to those in Fig. 3(b). Note, however, that the amplitude of the dynamical spin accumulation is much smaller than the spin accumulation of the steady-state spin transport shown by the dashed curve. The reason is that the AC drive oscillates too fast so that the spin accumulation does not have enough time to reach its steady-state value.

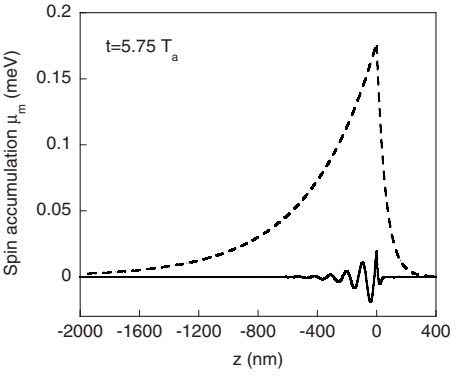

FIG. 4. Spin accumulation $\mu_m(z,t)$ for the same parameters as in Fig. 3(b).

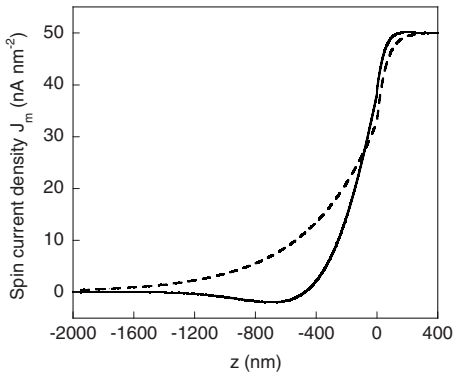

FIG. 5. Spin-current density $J_m(z,t)$ as a function of z. The solid curve is $J_m(z,t)$ at $t=1.75T_b$ [charge current $J(t)=-J_0$] with AC drive. The dashed curve is the spin-current density $J_m(z)$ for the case of a dc density $J=-J_0$.

Low-frequency case ($\omega=\omega_b<\omega_c$). Before analyzing the signal-propagation velocity, we first show how the results change qualitatively compared to the high-frequency case. In Fig. 5, the spin current J_m is plotted as a function of z driven by an AC with frequency ω_b, which is smaller than the critical frequency ω_c. The period T_b of the AC drive is 4.4 ps, which is much larger than T_a in Fig. 3. The solid curve is $J_m(z,t)$ at $t=1.75T_b$ (charge current $J=-J_0$) with AC drive. The dashed curve is again $J_m(z)$ driven by a constant current density $J=-J_0$. For this driving frequency, the wave character is insignificant because the wavelength $\lambda=1856$ nm becomes much larger than the damping length $l_d=268$ nm, and thus the wave amplitude is damped to zero within just one wavelength. From a practical point of view, the wavelength and the phase velocity $v_p=0.47c$ lose their meaning in this case. Comparison between the solid and dashed curves shows that the damping length for T_b becomes longer than that for T_a in Fig. 3, which is a consequence of the skin effect.

Figure 6 shows the spin accumulation μ_m as a function of z. The parameters used are the same as those in Fig. 5. The features of the spin accumulation are again reminiscent of the spin current in Fig. 5. Note that the spin accumulation has become larger compared to the AC drive with period T_a in Fig. 4. This is reasonable because the AC drive oscillates more slowly than that in Fig. 4, so that the spin accumulation has more time to approach its steady-state value.

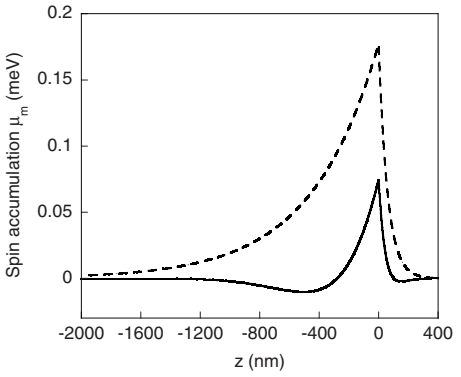

FIG. 6. Spin accumulation $\mu_m(z,t)$ for the same parameters as in Fig. 5.

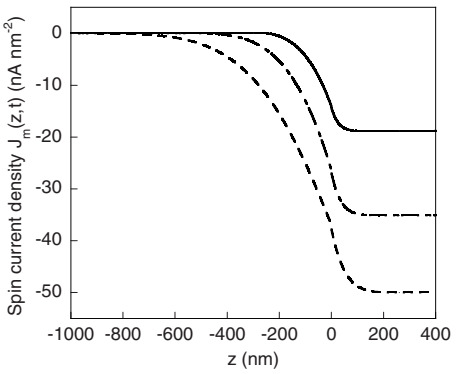

FIG. 7. Spin-current density $J_m(z,t)$ as a function of z. The solid, dot-dashed, and dashed curves are $J_m(z,t)$ at $t=T_b/16, T_b/8, T_b/4$, respectively, with ac drive.

At the time the snapshots in Figs. 5 and 6 are taken, no "wave front" of the spin current, or signal, can be distinguished. To determine the propagation velocity, we show $J_m(z,t)$ and $\mu_m(z,t)$ at $t=T_b/16$, $T_b/8$, and $T_b/4$ in Figs. 7 and 8, respectively. By tracking the motion of the wave front with time, we can estimate the propagation velocity of the signal. The result is in agreement with the wave-front velocity c, which according to our analysis of the telegraph equation [Eq. (23)] is still the propagation velocity.

Time-dependent spin transport in the low-frequency case can be described approximately by the conventional spin-diffusion equation. However, it is impossible to estimate the signal-propagation velocity from conventional spin-diffusion theory because there is no wave front in that case and the signal appears in infinity once the charge current $J(t)$ is switched on.[3,20]

B. Magnetization switching

The instantaneous switching of the magnetization in the ferromagnet, through which the current passes into the nonmagnetic metal, provides perhaps the conceptually cleanest picture of a spin-switching process. For a numerical study of this process, we consider again a ferromagnet/metal junction consisting of Co and Cu. We assume that the system is in a steady state in the presence of the dc drive with a charge

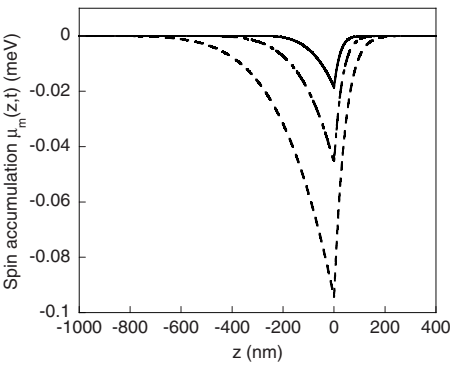

FIG. 8. Spin accumulation $\mu_m(z,t)$ for the same parameters as in Fig. 7.

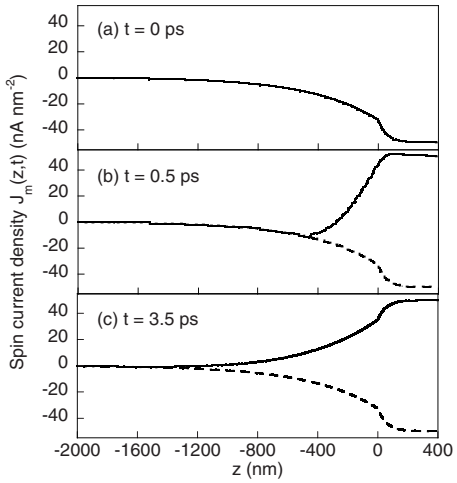

FIG. 9. Spin-current density $J_m(z,t)$ as a function of z. The solid curves in (a)–(c) are $J_m(z,t)$ at $t=0,0.5,3.5$ ps, respectively. The dashed curves in (b) and (c) are $J_m(z,t)$ at $t=0$ ps plotted again as a reference.

current density $J_0=100$ nA/nm^2 before the magnetization of the ferromagnetic layer is switched from up to down at $t=0$. We model the switching as an idealized instantaneous process and only consider the evolution of the spin-current density and spin accumulation afterwards. The spin-up electrons become the majority and the spin-down electrons become the minority after the instantaneous switching. The conductivities of the majority and minority channels are also exchanged by the switching. Although the evolution of $J_m(z,t)$ and $\mu_m(z,t)$ does not take the wave form used in Sec. III, it can be decomposed into different frequencies by Fourier transformation, so that the analysis of the telegraph equation still applies.

Figures 9 and 10 show the dynamics of the spin current and spin accumulation. Starting from the steady-state value shown in part (a), the magnetization is switched instantaneously at $t=0$. Figures 9(b) and 10(b) show snapshots 0.5 ps after the switch when a pronounced kink has developed. This kink indicates the leftmost position to which the magnetization-switching signal has propagated after 0.5 ps. The kink is noticeable only if the time t is so small that it does not propagate beyond the length scale of the spin-diffusion length l_{sf}, over which the steady-state signal decays. Thus the signal-propagation velocity can be estimated roughly by tracking the motion of the kink with time at the early stage of the switching. The result is very close to the wave-front velocity $c=910$ nm/ps calculated from the analytical result [Eq. (13)]. Moreover, Fig. 9(c) shows that the spin-current density reaches the steady state with down magnetization on the time scale of the spin-relaxation time T_1. Since $T_1 \gg \tau_s'$, we can consider $t=T_1$ as the long-time limit. This behavior is consistent with the result calculated from the diffusion equation in Ref. 3, so that again the diffusion character of spin transport emerges as an approximation of the wave-diffusion character in the long-time limit.

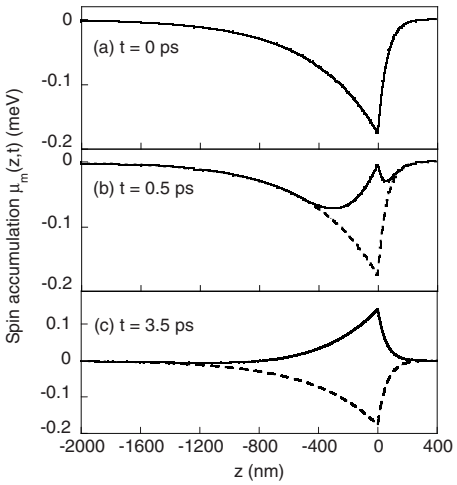

FIG. 10. Spin accumulation $\mu_m(z,t)$ for the same parameters as in Fig. 9.

V. SUMMARY

We studied signal propagation in time-dependent spin transport through magnetic multilayers using an extension of the Valet-Fert theory to time-dependent phenomena. We established that time-dependent spin transport has a wave character in addition to its diffusive character, which enabled us to determine the finite propagation velocity of signals in spin transport, such as ac spin injection and magnetization switching. The propagation velocity is the wave-front velocity $c=v_F/\sqrt{3}$. The wave character is significant if the signal time scale τ_{sig} is smaller than a critical time T_c. When the wave character is significant ($\tau_{sig}<T_c$), the time-dependent spin transport should be modeled by the dynamical equations introduced in this paper or, equivalently, the telegraph equations. However, pure diffusive spin transport can be regarded as an approximation of the wave-diffusion duality for slow switching times ($\tau_{sig}\gg T_c$). In this limit, the spin-diffusion equation can be used to study the time dependence of spin transport approximately, but it incorrectly yields an infinite signal-propagation velocity.

ACKNOWLEDGMENTS

We acknowledge financial support from the state of Rheinland-Pfalz through the MATCOR program and a CPU-time grant from the John von Neumann Institut for Computing (NIC) at the Forschungszentrum Jülich.

APPENDIX: IDENTITIES AND DERIVATIONS

1. Useful identities

Several useful identities will be established by the help of Eq. (3). Multiplying $\sin\theta$ and integrating over θ from 0 to π on both sides of Eq. (3), we have

$$\int_0^\pi d\theta \sin\theta g_s(z,\mathbf{v},t) = \sum_{n=1}^{\infty} g_s^{(n)}(z,t) \int_0^\pi d\theta \sin\theta P_n(\cos\theta). \tag{A1}$$

The right-hand side (RHS) of Eq. (A1) can be further written as

$$\mathrm{RHS} = \sum_{n=1}^{\infty} g_s^{(n)}(z,t) \int_{-1}^{1} du P_0(u) P_n(u). \tag{A2}$$

Using the orthogonality relation between Legendre polynomials,

$$\int_{-1}^{1} du P_{n'}(u) P_n(u) = \frac{2}{2n+1} \delta_{n,n'}, \tag{A3}$$

where $\delta_{n,n'}$ is the usual Kronecker symbol, we obtain from Eqs. (A1) and (A2)

$$\int_0^{\pi} d\theta \sin\theta g_s(z,\mathbf{v},t) = 0. \tag{A4}$$

Equation (A4) further leads to

$$\sum_{\mathbf{v}} g_s(z,\mathbf{v},t) = \frac{Vm^3}{h^3} \int d^3v g_s(z,\mathbf{v},t) = \frac{Vm^3}{h^3} \int_0^{2\pi} d\varphi \int_0^{\pi} d\theta \sin\theta \int_0^{\infty} dv v^2 g_s(z,\mathbf{v},t) = 0. \tag{A5}$$

2. Derivation of Eq. (4)

Following Ref. 11, we substitute Eq. (2) into Eq. (1) and use the following identity,

$$\frac{\partial f^0}{\partial \varepsilon} = \frac{1}{mv} \frac{\partial f^0}{\partial v} = \frac{-\delta(v - v_F)}{m v_F}. \tag{A6}$$

Then we can write the RHS (the collision terms) of Eq. (1) as

$$\begin{aligned} \frac{\partial f_s(z,\mathbf{v},t)}{\partial t}\Big|_{\mathrm{collision}} = & -\frac{\partial f^0(v)}{\partial \varepsilon} P_s[z,\varepsilon(v)] \frac{4\pi v}{m} \left[g_s(z,\mathbf{v},t) - \frac{1}{2} \int_0^{\pi} d\theta' \sin\theta' g_s(z,\mathbf{v}',t)\big|_{v'=v} \right] \\ & - \frac{\partial f^0(v)}{\partial \varepsilon} P_{\mathrm{sf}}[z,\varepsilon(v)] \frac{4\pi v}{m} \left[g_s(z,\mathbf{v},t) - \frac{1}{2} \int_0^{\pi} d\theta' \sin\theta' g_{-s}(z,\mathbf{v}',t)\big|_{v'=v} \right] \\ & + \frac{\partial f^0(v)}{\partial \varepsilon} P_{\mathrm{sf}}[z,\varepsilon(v)] \frac{4\pi v}{m} [\mu_s(z,t) - \mu_{-s}(z,t)]. \end{aligned} \tag{A7}$$

Using Eq. (A4), we can write Eq. (A7) in the form

$$\begin{aligned} \frac{\partial f_s(z,\mathbf{v},t)}{\partial t}\Big|_{\mathrm{collision}} = & -\frac{\partial f^0(v)}{\partial \varepsilon} P_s[z,\varepsilon(v)] \frac{4\pi v}{m} g_s(z,\mathbf{v},t) \\ & - \frac{\partial f^0(v)}{\partial \varepsilon} P_{\mathrm{sf}}[z,\varepsilon(v)] \frac{4\pi v}{m} g_s(z,\mathbf{v},t) \\ & + \frac{\partial f^0(v)}{\partial \varepsilon} P_{\mathrm{sf}}[z,\varepsilon(v)] \frac{4\pi v}{m} [\mu_s(z,t) \\ & - \mu_{-s}(z,t)]. \end{aligned} \tag{A8}$$

By introducing the relaxation times,

$$\frac{1}{\tau_s(v)} = P_s[z,\varepsilon(v)] \frac{4\pi v}{m}, \tag{A9}$$

$$\frac{1}{\tau_{\mathrm{sf}}(v)} = P_{\mathrm{sf}}[z,\varepsilon(v)] \frac{4\pi v}{m}, \tag{A10}$$

where the z dependence of the relaxation times is neglected within the same layer, we can further write Eq. (A8) as

$$\begin{aligned} \frac{\partial f_s(z,\mathbf{v},t)}{\partial t}\Big|_{\mathrm{collision}} = & -\frac{\partial f^0(v)}{\partial \varepsilon} \left(\frac{1}{\tau_s} + \frac{1}{\tau_{\mathrm{sf}}} \right) g_s(z,\mathbf{v},t) \\ & + \frac{\partial f^0(v)}{\partial \varepsilon} \frac{\mu_s(z,t) - \mu_{-s}(z,t)}{\tau_{\mathrm{sf}}}. \end{aligned} \tag{A11}$$

Taking into account the left-hand side of Eq. (1) and integrating over v, we can finally derive Eq. (4). Note that $\tau_s(v)$ and $\tau_{\mathrm{sf}}(v)$ are restricted to the Fermi velocity v_F after the integration over v and then they are simply written as τ_s and τ_{sf}.

3. Derivation of Eqs. (17) and (20)

Multiplying by $-e/V$ both sides of Eq. (2), summing over $\mathbf{v}$, and using Eq. (A5), we obtain

$$n_s(z,t) - n_s^0 = -eN_s[\mu_s(z,t) - \mu^0], \tag{A12}$$

where

$$n_s(z,t) = -\frac{e}{V} \sum_{\mathbf{v}} f_s(z,\mathbf{v},t), \tag{A13}$$

$$n_s^0 = -\frac{e}{V}\sum_{\mathbf{v}} f^0(v) = -en_s \tag{A14}$$

are the nonequilibrium and equilibrium charge densities for spin s, respectively. In turn, Eq. (A12) yields

$$n_m(z,t) = -eN_s\mu_m(z,t), \tag{A15}$$

$$n(z,t) - 2n_s^0 = -eN_s[2\mu(z,t) - 2\mu^0], \tag{A16}$$

where $n_m(z,t)=n_+(z,t)-n_-(z,t)$ is the spin density and $n(z,t)=n_+(z,t)+n_-(z,t)$ the total nonequilibrium charge density.

4. Numerical solution of Eqs. (10) and (11)

For the numerical solution of Eqs. (10) and (11) we use the method of characteristics and Hartree's computational form. Following Ref. 21, the space z and time t are discretized into grids with equal intervals Δz and Δt, respectively. The discretized forms of $J_m(z,t)$ and $\mu_m(z,t)$ are $J_{m,i}^n$ and $\mu_{m,i}^n$ at ith space point and nth time point, respectively. Then, $J_{m,i}^{n+1}$ and $\mu_{m,i}^{n+1}$ at $(n+1)$th time point can be calculated by the iteration relations,

$$\left(2+\frac{\Delta t}{T_1}\right)\mu_{m,i}^{n+1} = \left(1-\frac{\Delta t}{2T_1}\right)(\mu_{m,i-1}^n + \mu_{m,i+1}^n) - \frac{1}{eN_sc}\left(1-\frac{\Delta t}{2\tau}\right) \times (J_{m,i-1}^n - J_{m,i+1}^n), \tag{A17}$$

$$\left(2+\frac{\Delta t}{\tau}\right)J_{m,i}^{n+1} = -eN_sc\left(1-\frac{\Delta t}{2T_1}\right)(\mu_{m,i-1}^n - \mu_{m,i+1}^n) + \left(1-\frac{\Delta t}{2\tau}\right) \times (J_{m,i-1}^n + J_{m,i+1}^n) - \frac{\Delta t}{\tau}\tilde{\beta}(J^n + J^{n+1}), \tag{A18}$$

for all space points except the two boundary points, which should be determined by boundary conditions. Here, J^n is the total current density at nth time point. Moreover, Δz and Δt are chosen to satisfy the relation $\Delta z = c\Delta t$. Equations (A17) and (A18) can be iterated numerically to yield the results presented in Sec. IV. In the numerical solution, we used the following initial and boundary conditions for the AC spin injection and magnetization switching.

AC spin injection. The initial conditions are $\mu_m(z,t=0)=0$ and $J_m(z,t=0)=0$. The boundary condition for $\mu_m(z,t)$ is $\mu_m(z=\pm\infty,t)=0$. From Eq. (11), the boundary condition

$$J_m(z=\pm\infty,t) = \frac{\tilde{\beta}J_0}{1+\omega^2\tau^2}[\omega\tau\cos(\omega t) - \sin(\omega t) - \omega\tau\exp(-t/\tau)] \tag{A19}$$

for $J_m(z,t)$ can be derived.

Magnetization switching. The initial conditions for $J_m(z,t)$ and $\mu_m(z,t)$ are the steady-state solutions to Eqs. (10) and (11),

$$\mu_m^F(z,t=0) = C_0\exp(-z/l_{\mathrm{sf}}^F), \tag{A20}$$

$$J_m^F(z,t=0) = -\frac{C_0}{2e\rho_F^* l_{\mathrm{sf}}^F}\exp(-z/l_{\mathrm{sf}}^F) - \tilde{\beta}J_0, \tag{A21}$$

$$\mu_m^N(z,t=0) = C_0\exp(z/l_{\mathrm{sf}}^N), \tag{A22}$$

$$J_m^N(z,t=0) = \frac{C_0}{2e\rho_N^* l_{\mathrm{sf}}^N}\exp(z/l_{\mathrm{sf}}^N), \tag{A23}$$

where $C_0=-2e\tilde{\beta}J_0(\rho_F^* l_{\mathrm{sf}}^F\rho_N^* l_{\mathrm{sf}}^N)/(\rho_F^* l_{\mathrm{sf}}^F+\rho_N^* l_{\mathrm{sf}}^N)$. Here, μ_m^F and J_m^F apply to the ferromagnetic layer occupying $z>0$, whereas μ_m^N and J_m^N refer to the nonmagnetic layer $(z<0)$. In deriving the initial conditions above, we have used the identity $1/(2\rho_{N(F)}^*)=\sigma_{N(F)}/2=e^2N_s\bar{D}_{N(F)}$, where $\sigma_{N(F)}$ is the total conductivity of the nonmagnetic (ferromagnetic) layer. The boundary condition for $\mu_m(z,t)$ is $\mu_m(z=\pm\infty,t)=0$. Then, the boundary condition for $J_m(z,t)$ can again be derived from Eq. (11). This yields

$$J_m(z=\pm\infty,t) = \tilde{\beta}J_0[1-2\exp(-t/\tau)], \tag{A24}$$

where $\tilde{\beta}$ is the asymmetry parameter before the magnetization switching. Note that $\tilde{\beta}$ becomes $-\tilde{\beta}$ when the magnetization is switched $(t>0)$.

*hcsch@physik.uni-kl.de

[1] I. Žutić, J. Fabian, and S. D. Sarma, Rev. Mod. Phys. **76**, 323 (2004).
[2] J. Fabian, A. Matos-Abiague, C. Ertler, P. Stano, and I. Žutić, Acta Phys. Slov. **57**, 565 (2007).
[3] S. Zhang and P. M. Levy, Phys. Rev. B **65**, 052409 (2002).
[4] E. I. Rashba, Appl. Phys. Lett. **80**, 2329 (2002).
[5] J. Zhang and P. M. Levy, Phys. Rev. B **71**, 184417 (2005).
[6] Ł. Cywiński, H. Dery, and L. J. Sham, Appl. Phys. Lett. **89**, 042105 (2006).
[7] J. C. Maxwell, Philos. Trans. R. Soc. London **157**, 49 (1867).
[8] G. Cattaneo, Atti Semin. Mat. Fis. Univ. Modena **3**, 83 (1948).
[9] D. D. Joseph and L. Preziosi, Rev. Mod. Phys. **61**, 41 (1989).
[10] J. A. Scales and R. Snieder, Nature (London) **401**, 739 (1999).
[11] T. Valet and A. Fert, Phys. Rev. B **48**, 7099 (1993).
[12] In general, $E(z,t)$ is related to the scalar potential V and vector potential $\mathbf{A}$ by $\mathbf{E}=-\nabla V(z,t)-\partial\mathbf{A}/\partial t$. However, using a gauge transformation one can achieve $E(z,t)=-\partial V(z,t)/\partial z$ cf. Refs. 3–6.
[13] A. Fert and S.-F. Lee, Phys. Rev. B **53**, 6554 (1996).
[14] M. Chester, Phys. Rev. **131**, 2013 (1963).
[15] A. M. Kadin, L. N. Smith, and W. J. Skocpol, J. Low Temp. Phys. **38**, 497 (1980).
[16] N. W. Ashcroft and N. D. Mermin, *Solid State Physics* (Brooks/Cole, Belmont, CA, 1976).
[17] Q. Yang, P. Holody, S.-F. Lee, L. L. Henry, R. Loloee, P. A. Schroeder, W. P. Pratt, Jr., and J. Bass, Phys. Rev. Lett. **72**, 3274 (1994).
[18] L. Piraux, S. Dubois, A. Fert, and L. Belliard, Eur. Phys. J. B **4**, 413 (1998).
[19] S. Hershfield and H. L. Zhao, Phys. Rev. B **56**, 3296 (1997).
[20] J. Masoliver and G. H. Weiss, Eur. J. Phys. **17**, 190 (1996).
[21] W. F. Ames, *Numerical Methods for Partial Differential Equations*, 3rd ed.(Academic, San Diego, CA, 1992), see Sec. 4–15.